

# A Fabry–Perot Interferometer With Asymmetrical Tapered-Fiber for Improving Strain Sensitivity

Yanping Chen, Junxian Luo, Shen Liu , Mengqiang Zou, Shengzhen Lu, Yong Yang, Changrui Liao ,  
Wenjie Feng , and Yiping Wang 

**Abstract**—An effective method, reducing the material volume of the air cavity by asymmetrical tapering fiber, is demonstrated to enhance the sensitivity of the strain sensor dramatically. High-sensitive strain sensors are fabricated through this method that splicing and tapering fiber with arc discharge at the misaligned center of the air cavity. The strain sensitivity of the sensor is measured to be  $\sim 41.81$  pm/ $\mu\epsilon$  at a resonant wavelength  $\sim 1560$  nm ranging from 0 to 500  $\mu\epsilon$ . In addition, the experimental results show that the asymmetrical tapered-fiber enables both the material volume to smaller and the wall thickness to thinner, resulting in strain sensitivity higher. The proposed sensors have the advantages of fabricated repeatability, high sensitivity, and compact size, benefiting its practical sensing applications.

**Index Terms**—Fabry–Perot interferometer, fiber optics sensors, strain sensor.

## I. INTRODUCTION

**O**PTICAL fiber sensors for strain sensing applications have attracted great interest due to their advantages of simple configuration, compact size, low-temperature cross-sensitivity, and high sensitivity [1], [2]. They generally fall into the following categories, such as fiber Bragg grating (FBG) sensor [3]–[6], Mach-Zehnder interferometer (MZI) fiber sensor [7]–[10], Fabry-Perot interferometer (FPI) fiber sensor [11]–[15], and Sagnac interferometric configuration [16]. The strain sensitivities of these sensor schemes were typically about 1 pm/ $\mu\epsilon$  for FBGs, less than 10 pm/ $\mu\epsilon$  for MZIs, and less than

16 pm/ $\mu\epsilon$  for FPIs [17]. Moreover, the cross-sensitivity between strain and temperature was hardly overcome in these sensor schemes except for FPIs. Thus a few methods have been reported fabricating FPIs fiber sensor. Typically, methods of creating in-fiber air cavities have been widely studied, such as using silica hollow tube [18], [19] or photonic crystal fibers (PCFs) [20], direct micromachining using focused femtosecond laser beam along with splicing [21], chemical etching [22] *et al.* To enhance the strain sensitivity of fiber sensors based on FPIs, some additional designs have been demonstrated. For example, Zhang *et al.* [23] reported an FPI consisting of two cascaded air cavities, forming a Vernier effect, and achieving a strain sensitivity of 47.14 pm/ $\mu\epsilon$ . Liu *et al.* [24] proposed to fabricate a rectangular-shape air cavity with a wall thickness of about 1  $\mu\text{m}$  using techniques of splicing and tapering, achieving a strain sensitivity as high as 43.0 pm/ $\mu\epsilon$ . In addition, special optical fiber structures were employed to enhance the strain sensitivity. Zhang *et al.* [17] introduced helical structures (HSs) into a multicore fiber (MCF), achieving a maximum strain sensitivity as high as  $-61.8$  pm/ $\mu\epsilon$ . However, all these techniques above require expensive equipment, complicated fabrication process, expensive PCFs, and/or other special optical fibers.

In this paper, we demonstrate an effective method to achieve high strain sensitivity by fabricating an air cavity in an asymmetrical tapered single-mode fiber (SMF, Corning Inc., SMF-28.). The strain sensor is fabricated through the technique of splicing and followed by a tapering process, i.e., repeating arc-discharge at the misaligned center of the air cavity. The silica material of the in-fiber air cavity is partly reduced during the fiber-tapering process, i.e., reducing the material volume that results in thinning the wall thickness of the air cavity gradually. A series of high-sensitive strain sensors, with asymmetrical tapered-fiber and thin wall thickness, are fabricated successfully through the method mentioned above. Here, the structure size of the sensor, i.e., wall thickness, air cavity radius, can be precisely controlled through employing different values of fusion power, fusion time, and axial tensile stress. The strain sensitivity of one sensor sample is measured to be about 41.81 pm/ $\mu\epsilon$  at the resonant wavelength of about 1560 nm, with a sensing range of 0 to 500  $\mu\epsilon$ . In addition, the experimental measurements reveal that the asymmetrical tapered-fiber enables the wall thickness of the air cavity to thinner, resulting in strain sensitivity higher. Since the proposed sensor has advantages of fabricated repeatability, high sensitivity, and compact size, thereby enabling a wide spectrum of applications.

Manuscript received September 8, 2020; revised October 11, 2020; accepted November 5, 2020. Date of publication November 10, 2020; date of current version March 1, 2021. This work was supported in part by the National Natural Science Foundation of China (NSFC) under Grant 61905165 and Grant 61635007, in part by the Natural Science Foundation of Guangdong Province under Grant 2019A050510047 and Grant 2019B1515120042; in part by the Education Department of Guangdong Province under Grant 2018KQNCX219; and in part by the Science and Technology Innovation Commission of Shenzhen under Grant JCYJ20170412105604705, Grant JCYJ20180305125352956, and Grant JCYJ20170818093743767. (Corresponding author: Shen Liu.)

Yanping Chen, Junxian Luo, Shen Liu, Mengqiang Zou, Shengzhen Lu, Yong Yang, Changrui Liao, and Yiping Wang are with the Shenzhen Key Laboratory of Photonic Devices and Sensing Systems for Internet of Things, College of Physics and Optoelectronic Engineering, Shenzhen University, Shenzhen 518060, China, and also with the Guangdong and Hong Kong Joint Research Centre for Optical Fibre Sensors, Shenzhen University, Shenzhen 518060, China (e-mail: chongyouchenyp@sina.com; 479504814@qq.com; shenliu@szu.edu.cn; mengqiangzou@163.com; rosejenny73@163.com; yangy79@gmail.com; cliao@szu.edu.cn; ypwang@szu.edu.cn).

Wenjie Feng is with the Department of Communication Engineering, Nanjing University of Science & Technology, Nanjing 210094, China (e-mail: fengwenjie1985@163.com).

Color versions of one or more of the figures in this article are available online at <https://ieeexplore.ieee.org>.

Digital Object Identifier 10.1109/JLT.2020.3037178

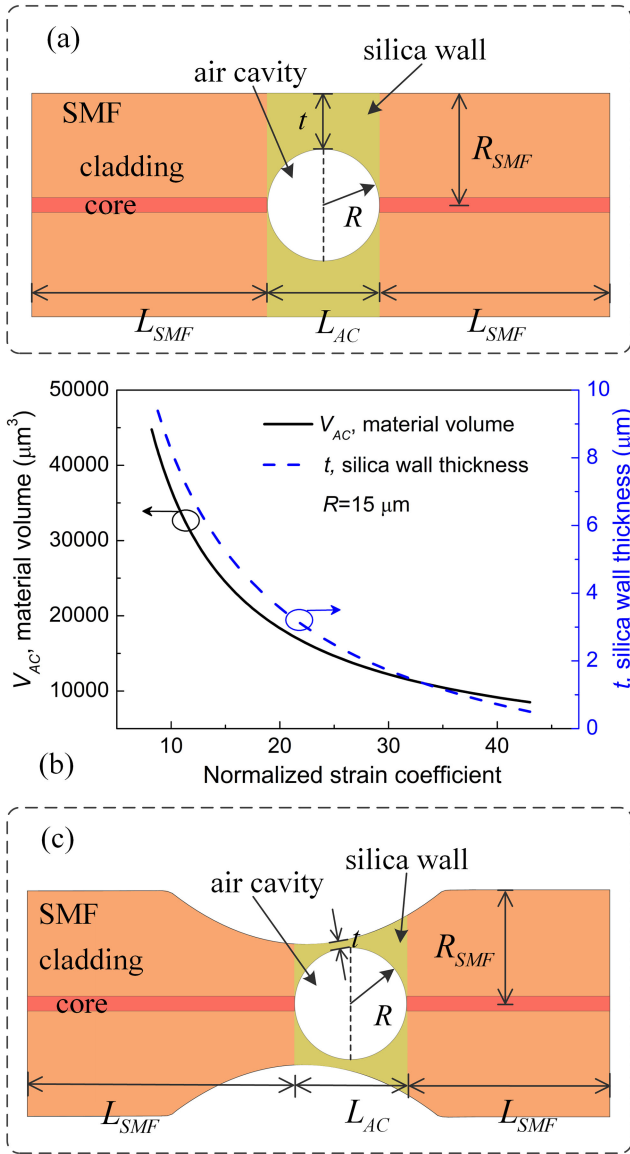


Fig. 1. (a) Schematic diagram of an in-fiber FPI strain sensor based on an air cavity. (b) Calculated normalized strain coefficient variation with material volume and silica wall thickness of the air cavity. (c) Optimized schematic of an in-fiber FPI strain sensor based on an air cavity with an asymmetrical tapered-fiber.

## II. ANALYSIS OF STRAIN SENSITIVITY ENHANCEMENT

Fig. 1(a) illustrates the schematic of an in-fiber FPI strain sensor based on an air cavity. Strain is applied to the sensor, of which measured total length can be written as  $L_{total} = L_{AC} + L_{SMF}$ , where  $L_{AC}$  and  $L_{SMF}$  are the air cavity length, and the measured SMF length, respectively. Considering that strain is applied at a constant temperature to the air cavity of the FPI, the shift of interference fringes  $\Delta\lambda_{AC}$  is recorded as,

$$\Delta\lambda_{AC} = k_{\varepsilon(AC)}\varepsilon_{AC} \quad (1)$$

where,  $k_{\varepsilon(AC)}$  and  $\varepsilon_{AC}$  are the strain coefficient and the applied strain, respectively. When stress is applied to the entire sensor, each section of the sensor will suffer an unequal load of strain,

depending on the local mechanical resistance. The strain loads applied to the air cavity and the SMF are equal, as

$$\varepsilon_{AC}EA_{AC} = \varepsilon_{SMF}EA_{SMF} \quad (2)$$

where  $E$  is Young modulus of the fiber material, and  $A_{AC}$  and  $A_{SMF}$  are the cross sections of the fiber material areas of air cavity and the SMF, respectively. As shown in Fig. 1(a),  $A_{SMF} = \pi(R_{SMF})^2$ , and  $R_{SMF}$  is the SMF's radius. The details behind the equations here summarized can be found in Ref. [6]. After some algebraic manipulation, the normalized strain coefficient related to the material volume of the air cavity can be written as

$$\begin{aligned} \frac{k_{\varepsilon(AC)}}{k_{\varepsilon 0}} &= \frac{L_{AC} + L_{SMF}}{L_{AC} + L_{SMF} \frac{V_{AC}}{L_{AC} \cdot A_{SMF}}} \\ &= \frac{L_{AC} + L_{SMF}}{L_{AC} + L_{SMF} \frac{V_{AC}}{V_{SMF(AC)}}} \end{aligned} \quad (3)$$

where,  $k_{\varepsilon 0}$  is the strain coefficient when the material section area of the air cavity is equal to the SMF section area, and  $V_{SMF(AC)}$  denotes the SMF material volume with a length of  $L_{AC}$ , and  $V_{AC}$  is the material volume of the air cavity, and is calculated by

$$V_{AC} = L_{AC}\pi(R+t)^2 - \frac{4}{3}\pi R^3 \quad (4)$$

where,  $t$  is the thinnest silica wall thickness of the air cavity,  $R$  is the radius of the air cavity. Fig. 1(b) shows the dependence of the air cavity strain coefficient on the material volume and silica wall thickness, in black solid and blue dotted lines, respectively. The air cavity radius  $R = 15 \mu\text{m}$ , the SMF's radius  $R_{SMF} = 62.5 \mu\text{m}$ , the total length  $L_{total} = 200 \text{ mm}$ , and the air cavity length  $L_{AC} = 2 \times R = 30 \mu\text{m}$ . It can be seen that a significant increase in the strain sensitivity when a large decrease of the air cavity material volume or the silica wall thickness. Thus, reducing the material volume or the silica wall thickness of the air cavity can effectively improve the strain sensitivity. As shown in Fig. 1(c), the in-fiber FPI strain sensor, based on an air cavity, is optimized with an asymmetrical tapered-fiber. It is clearly seen that both the material volume and the silica wall thickness of the air cavity are effectively reduced as compared to that in Fig. 1(a), thus the strain sensitivity can be improved significantly.

## III. ENHANCING STRAIN SENSITIVITY BY FABRICATING ASYMMETRICAL TAPERED-FIBER

Fig. 2 illustrates the fabrication process of the in-fiber FPI based on an air cavity with an asymmetrical tapered-fiber, which involves two steps. In step 1, as shown in Fig. 2(a), the in-fiber air cavity with two fiber ends was placed in the left and right fiber holders of a commercial fusion splicer, respectively. One of the two fiber ends was moved away from the other one via the left or the right motor of the fusion splicer, where  $d$  indicates the moved distance of the left or the right fiber end. In step 2, as shown in Fig. 2(b), the fiber segment with the air cavity was tapered by electrical arc-discharge at the misaligned center of the air cavity, with fusion power of standard and fusion time of  $\sim 750 \text{ ms}$ . Consequently, an asymmetrical tapered-fiber was induced in the fiber segment, resulting from the pre-stress of the fiber ends. The

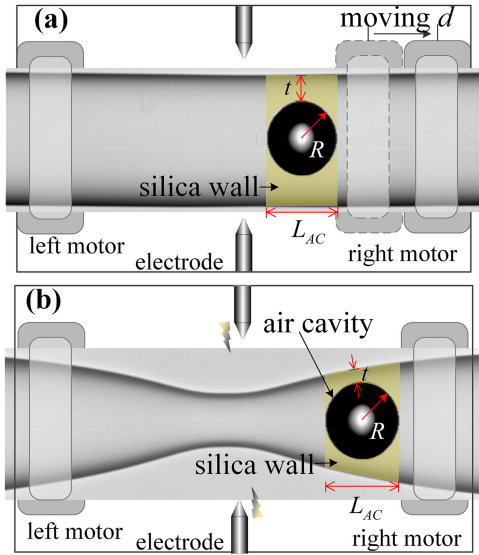


Fig. 2. Fabrication process of misaligned arc-discharge at the center of the air cavity.

silica material of the air cavity was partly reduced during the fiber-tapering process, reducing both the material volume and the wall thickness of the air cavity gradually. Compared with the technique reported in Ref. [24], i.e., electrical arc discharge implemented at the middle of air bubble, the fabrication process of the asymmetrical fiber strain sensor is more effective and simpler. Note that, the manual operation mode of the fusion splicer (Fujikura, FSM-60S) was used to fabricate the air cavity samples; all the sizes of the structure, including the wall thickness and the air cavity radius, can be precisely controlled through employing different values of fusion power, fusion time, and axial tensile stress. In addition, in the whole fabrication process, only a common fusion splicer was employed, and no additional device was required. Detailed processes related to air cavity fabrication are well described in previous studies [1], [24].

Fig. 3 shows the optical microscope images and the corresponding reflection spectra of two in-fiber FPI strain sensors based on an air cavity with an asymmetrical tapered-fiber. Sample-1 and sample-2 with different taper waists of 22.8 and 51  $\mu\text{m}$ , and different air cavity lengths of 30 and 57  $\mu\text{m}$ , are shown in Figs. 3(a) and 3(c), respectively. A broadband light source (ASE LIGHG SOURCE), a 3-dB fiber coupler, and an optical spectrum analyzer (OSA, YOKOGAWA AQ6370C) with a resolution of 0.02 nm were employed to measure the reflection spectra of these two samples. The corresponding reflection spectra of sample-1 and sample-2 are illustrated in Figs. 3(b) and 3(d), respectively. Their corresponding free spectral ranges (FSRs) are  $\sim 41$  and  $\sim 22.1$  nm, and the extinction ratios (ERs) are 17.9 and 29.85 dB, respectively.

#### IV. STRAIN SENSING AND DISCUSSION

To investigate the strain sensitivity of the FPI based on an air cavity with an asymmetrical tapered-fiber, two samples shown in Fig. 3 were tested. Each sample has a tapered structure and

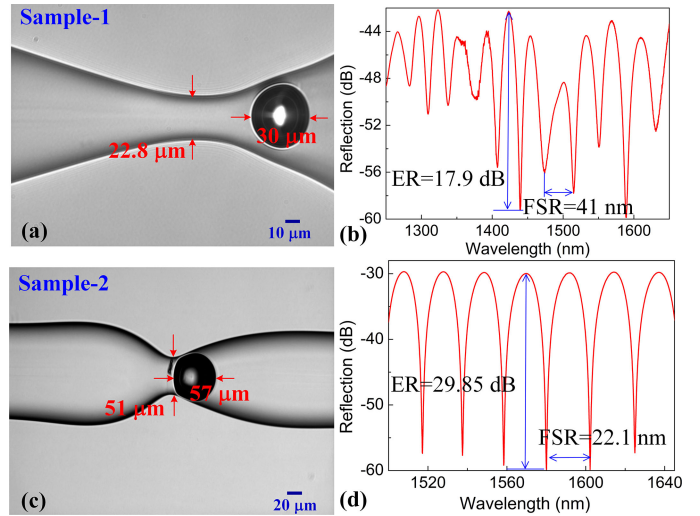


Fig. 3. Microscope images of the in-fiber FPI with a cavity length of (a)  $\sim 30$   $\mu\text{m}$  and (c)  $\sim 57$   $\mu\text{m}$  in an asymmetrical tapered fiber. The corresponding original reflection spectra of (b) sample-1 and (d) sample-2.

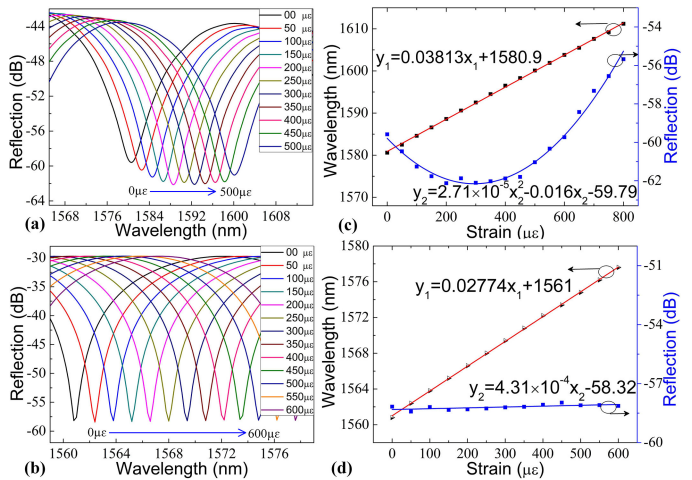


Fig. 4. Strain response of the two air cavity samples. (a) and (b) Reflection spectrum evolution of the air cavity-based FPI samples, i.e., (a) sample-1, while the tensile strain increases from 0 to 500  $\mu\epsilon$ , and (b) sample-2, while the tensile strain increases from 0 to 600  $\mu\epsilon$ . (c) and (d) Wavelength shift of interference fringe around 1580 nm and 1560 nm as a function of tensile strain applied to (c) sample-1 and (d) sample-2, respectively.

a thin wall thickness. Sample-1 in Fig. 3(a) has a shorter cavity length and a thicker wall thickness compared to the sample-2 in Fig. 3(c). One end of the air cavity was fixed and glued on a holder, and the other end was firmly attached to a translation stage with a resolution of 10  $\mu\text{m}$ . The total length of the stretched fiber, including the SMF and in-fiber air cavity, is 200 mm. A tensile strain was applied to the air cavity sample by moving the translation stage away from the fixed one at room temperature. As shown in Figs. 4(a) and 4(b), the dip wavelength shift of the reflection fringe around 1580 nm for sample-1 and around 1560 nm for sample-2 were measured while the tensile strain was increased from 0 to 500  $\mu\epsilon$  and 0 to 600  $\mu\epsilon$  with a step of 50  $\mu\epsilon$ , respectively. The fringe dips of the two samples shifted linearly

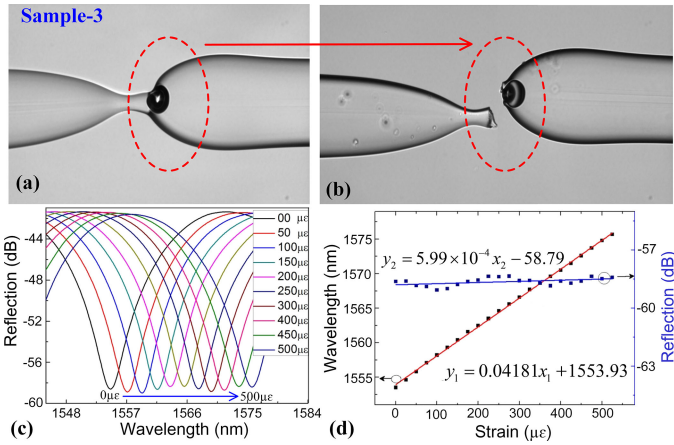


Fig. 5. (a) Microscope image of the in-fiber FPI with a cavity length of  $\sim 20 \mu\text{m}$  in an asymmetrical tapered fiber. (b) Microscope image of the in-fiber FPI with fracture surface appears in the fiber. (c) Reflection spectrum evolution of the air cavity-based FPI sample-3 while the tensile strain increases from 0 to  $500 \mu\epsilon$ . (d) Wavelength shift of interference fringe around  $1555 \text{ nm}$  as a function of tensile strain applied to sample-3.

toward a longer wavelength as the tensile strain increasing are shown in Figs. 4(c) and 4(d), respectively. The strain sensitivity of sample-1 and sample-2 was calculated to be  $38.13$  and  $27.74 \text{ pm}/\mu\epsilon$ , respectively, by linear fitting the dip wavelength change of the experimental data. The strain sensitivity of the air cavity samples with asymmetrical tapered-fiber, i.e., sample-1 and sample-2, is almost nine and six times higher than that of the air cavity sample with a cavity length  $58 \mu\text{m}$  reported in Ref. [1], respectively, which indicates that the asymmetrical tapered-fiber can significantly enhance the strain sensitivity of the air-cavity-based FPI. In addition, Sample-1 has higher strain sensitivity as compared to sample-2, the reason is sample-1 has a shorter air cavity length as compared to sample-2, and the decrease of the air cavity length enables higher strain sensitivity [1].

In addition, we recorded the dip values of the air cavities' reflection spectra, shown in Figs. 4(c) and 4(d) in blue dots, respectively. The fringe contrast has some certain variations for sample-1. The reason might be the inner wall of the air cavity for sample-1 is sensitive to tensile strain, for the increased tensile strain will change the flatness of the inner wall of the air cavity. The reflectivity of the two inner walls of sample-2 will hardly be changed as the tensile strain increases because these inner walls are well protected in the fiber.

Although the proposed FPI strain sensor based on an air cavity with asymmetrical tapered-fiber shows high strain sensitivity, it has limitations regarding mechanical robustness. Typically, a proposed strain sensor sample-3 with an asymmetrical tapered-fiber is shown in Fig. 5(a). The strain sensitivity of this sample was tested, and the reflection spectrum evolution is shown in Fig. 5(c). And the strain sensitivity is calculated to be  $41.81 \text{ pm}/\mu\epsilon$  by applying a linear fitting of the experimental data, as shown in Fig. 5(d). The tensile strength of the sample-3 is investigated by continuously increases the tensile strain to the sample until the tested sample breaks into two sections. In the process of applying  $550 \mu\epsilon$  axial strain to the FPI, the main part

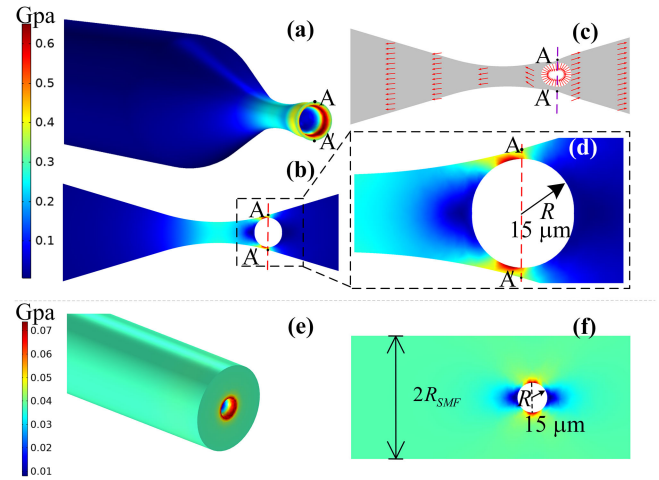


Fig. 6. Three-dimensional stress distribution contours while axial strain of  $500 \mu\epsilon$  applied to the model (a) with tapered-fiber and (e) without tapered-fiber. (b), (f) The corresponding stress distributions along the transverse section for the model (b) with tapered-fiber and (f) without tapered-fiber. (d) Enlarged partial view of the air cavity of (b). (c) The corresponding deformation along the transverse section for the model with tapered-fiber.

of the FPI is torn. The reason might be the tensile strength of the in-fiber FPI strain sensor based on an air cavity with asymmetrical tapered-fiber is lower than that without the asymmetrical structure. Thus, high strain sensitivity is achieved by sacrificing the tensile strength, and a good balance between strain sensitivity and robustness should be made in the air-cavity-based sensor design. The microscope image of the broken in-fiber FPI is shown in Fig. 5(b).

To investigate the stress distribution and the deformation on the sensor under an applied tensile strain, the model of the air cavity with an asymmetrical tapered-fiber is established and shown in Fig. 6(a). The standard parameters are employed in the simulations, i.e., silica density of  $2700 \text{ kg}/\text{m}^3$ , Young's modulus of  $73 \text{ GPa}$ , and Poisson's ratio of  $0.17$  [24]. The simulation model is established using the values measured from the optical microscope images of sample-1 shown in Fig. 3(a). Fig. 6(a) illustrates the three-dimensional stress distribution contour of the strain sensor, with a tensile strain of  $500 \mu\epsilon$ , and the colors indicate the stress distribution in different parts of the strain sensor. It is observed that the maximum stress is distributed on the surface of the air cavity, where the silica wall thickness is the thinnest, as shown in Figs. 6(b) and 6(d). The vector displacement contours are shown in Fig. 6(c), and the arrows describe the directions of the sensor's deformation. At the marked points A and A' on the equator surface of the air cavity in Fig. 6(c), it is observed that the marked points shift toward the inner center of the air cavity, indicating that the equatorial radius is reduced.

For comparison, another in-fiber FPI strain sensor based on an air cavity without asymmetrical tapered-fiber was established, as shown in Fig. 6(e). The diameter of the air cavity is the same as that in the model shown in Fig. 6(a). When the axial strain of  $500 \mu\epsilon$  is applied to this model, the simulated 2D stress contour of the air cavity is shown in Fig. 6(f). As shown in Figs. 6(d) and 6(f), the value of stress distribution on the thinnest wall thickness of

the air cavity is the largest, which agrees with the results reported in previous studies in Ref. [24]. Moreover, compare the model shown in Figs. 6(a) and 6(e), it is observed that the model with asymmetrical tapered-fiber concentrates much more stress.

## V. CONCLUSION

The strain sensitivity is proved to be related to both the material volume and the wall thickness of the air cavity. An effective method, reducing the material volume of the air cavity by asymmetrical tapering fiber, is demonstrated to enhance the sensitivity of the strain sensor dramatically. The fabrication method consists of fusion splicing and a tapering process, which is realized through repeating arc-discharge at the misaligned center of the air cavity. The strain sensitivity of one sensor sample is measured to be  $\sim 41.81 \text{ pm}/\mu\epsilon$  at the resonant wavelength of about 1560 nm, with a sensing range of 0 to 500  $\mu\epsilon$ . Such a strain sensor has the advantages of fabricated repeatability, high sensitivity, compact size, and low cost. It is promising for highly sensitive strain sensing in practical harsh environments.

## REFERENCES

- [1] S. Liu *et al.*, "High-sensitivity strain sensor based on in-fiber improved Fabry–Perot interferometer," *Opt. Lett.*, vol. 39, no. 7, pp. 2121–2124, Apr. 2014.
- [2] Y. Wu, Y. Zhang, J. Wu, and P. Yuan, "Fiber-Optic hybrid-structured fabry–perot interferometer based on large lateral offset splicing for simultaneous measurement of strain and temperature," *J. Lightw. Technol.*, vol. 35, no. 19, pp. 4311–4315, Oct. 2017.
- [3] J. Villatoro *et al.*, "Accurate strain sensing based on super-mode interference in strongly coupled multi-core optical fibres," *Scientific Rep.*, vol. 7, Jun. 2017, Art. no. 4451.
- [4] I. C. Song, S. K. Song, S. H. Jeong, and B. H. Lee, "Absolute strain measurements made with fiber bragg grating sensors," *Appl. Opt.*, vol. 43, no. 6, pp. 1337–1441, Feb. 2004.
- [5] R. Oliveira, L. Bilro, T. H. R. Marques, C. M. B. Cordeiro, and R. Nogueira, "Strain sensitivity enhancement of a sensing head based on ZEONEX polymer FBG in series with silica fiber," *J. Lightw. Technol.*, vol. 36, no. 22, pp. 5106–5112, Nov. 2018.
- [6] O. Frazao, S. F. O. Silva, A. Guerreiro, J. L. Santos, L. A. Ferreira, and F. M. Araujo, "Strain sensitivity control of fiber bragg grating structures with fused tapers," *Appl. Opt.*, vol. 46, no. 36, pp. 8578–8582, Nov. 2007.
- [7] P. Lu, L. Men, K. Sooley, and Q. Chen, "Tapered fiber Mach–Zehnder interferometer for simultaneous measurement of refractive index and temperature," *Appl. Phys. Lett.*, vol. 94, no. 13, Apr. 2009, Art. no. 131110.
- [8] H. Y. Choi, M. J. Kim, and B. H. Lee, "All-fiber Mach–Zehnder type interferometers formed in photonic crystal fiber," *Opt. Express*, vol. 15, no. 9, pp. 5711–5720, Apr. 2007.
- [9] C. Liao, D. Wang, and Y. Wang, "Microfiber in-line Mach–Zehnder interferometer for strain sensing," *Opt. Lett.*, vol. 38, no. 5, pp. 757–759, Mar. 2013.
- [10] P. Lu and Q. Chen, "Asymmetrical fiber Mach–Zehnder interferometer for simultaneous measurement of axial strain and temperature," *IEEE Photon. J.*, vol. 2, no. 6, pp. 942–953, Dec. 2010.
- [11] H. F. Chen, D. N. Wang, and Y. Wang, "Simultaneous strain and temperature sensing using a slightly tapered optical fiber with an inner cavity," *Analyst*, vol. 140, no. 6, pp. 1859–1862, 2015.
- [12] M. S. Ferreira, J. Bierlich, J. Kobelke, K. Schuster, J. L. Santos, and O. Frazão, "Towards the control of highly sensitive Fabry–Pérot strain sensor based on hollow-core ring photonic crystal fiber," *Opt. Express*, vol. 20, no. 20, pp. 21946–21952, Sep. 2012.
- [13] J. Tian *et al.*, "A Fabry–Pérot interferometer strain sensor based on concave-core photonic crystal fiber," *J. Lightw. Technol.*, vol. 36, no. 10, pp. 1952–1958, May 2018.
- [14] M. Deng, T. Zhu, and Y. Rao, "PCF-Based Fabry–Pérot interferometric sensor for strain measurement at high temperatures," *IEEE Photon. Technol. Lett.*, vol. 23, no. 11, pp. 700–702, Jun. 2011.
- [15] Y. Zhao, M. Chen, and Y. Peng, "Tapered hollow-core fiber air-microbubble Fabry–Perot interferometer for high sensitivity strain measurement," *Adv. Mater. Interfaces*, vol. 5, Nov. 2018, Art. no. 1800886.
- [16] X. Dong, H. Y. Tam, and P. Shum, "Temperature-insensitive strain sensor with polarization-maintaining photonic crystal fiber based sagnac interferometer," *Appl. Phys. Lett.*, vol. 90, no. 15, Apr. 2007, Art. no. 151113.
- [17] H. Zhang *et al.*, "Highly sensitive strain sensor based on helical structure combined with Mach–Zehnder interferometer in multicore fiber," *Scientific Rep.*, vol. 7, no. 1, Apr. 2017, Art. no. 46633.
- [18] G. K. B. Costa, P. M. P. Gouvêa, L. M. B. Soares, J. M. B. Pereira, and I. C. S. Carvalho, "In-fiber Fabry–Perot interferometer for strain and magnetic field sensing," *Opt. Express*, vol. 24, no. 13, Jun. 2016, Art. no. 14690.
- [19] Y. Wu, Y. Zhang, J. Wu, and P. Yuan, "Temperature-insensitive fiber optic Fabry–Perot interferometer based on special air cavity for transverse load and strain measurements," *Opt. Express*, vol. 25, no. 8, pp. 9443–9448, Apr. 2017.
- [20] X. Xi, G. K. L. Wong, T. Weiss, and P. S. J. Russell, "Measuring mechanical strain and twist using helical photonic crystal fiber," *Opt. Lett.*, vol. 38, no. 24, pp. 5401–5404, Dec. 2013.
- [21] C. Zhang, S. Fu, M. Tang, and D. Liu, "Parallel Fabry–Perot interferometers fabricated on multicore-fiber for temperature and strain discriminative sensing," *Opt. Express*, vol. 28, no. 3, pp. 3190–3199, Feb. 2020.
- [22] P. Zhang, L. Zhang, Z. Wang, X. Zhang, and Z. Shang, "Sapphire derived fiber based Fabry–Perot interferometer with an etched micro air cavity for strain measurement at high temperatures," *Opt. Express*, vol. 27, no. 19, Sep. 2019, Art. no. 27112.
- [23] P. Zhang *et al.*, "Cascaded fiber-optic Fabry–Perot interferometers with vernier effect for highly sensitive measurement of axial strain and magnetic field," *Opt. Express*, vol. 22, no. 16, Aug. 2014, Art. no. 19581.
- [24] S. Liu *et al.*, "High-sensitivity strain sensor based on in-fiber rectangular air bubble," *Scientific Rep.*, vol. 5, no. 1, Jan. 2015, Art. no. 7624.

**Yanping Chen** was born in Chongqing, China, in 1990. She received the M.S. degree in optical engineering from the Chongqing University of Posts and Telecommunications in 2016. She is currently working toward the Ph.D. degree in optical engineering with Shenzhen University, Shenzhen, China.

**Junxian Luo** was born in Guangxi, China, in 1996. She received the B.S. degree in optoelectronic information science technology and engineering from the Guilin University of Electronic Technology in 2018. Her current research interests focus on optical fiber resonator and phase-shifted Bragg grating based on femtosecond laser micro-processing technology.

**Shen Liu** was born in Henan, China, in 1986. He received the M.S. degree in circuit and system from the Chongqing University of Posts and Telecommunications in 2013, and the Ph.D. degree in optical engineering from Shenzhen University, Shenzhen, China, in 2017. From 2017 to 2018, he was with Aston University, Birmingham, U.K., as a Postdoctoral Fellow. Since 2018, he has been with Shenzhen University, as an Assistant Professor. He has authored or coauthored 11 patent applications and more than 30 journal and conference papers. His current research interests focus on optical fiber sensors, WGMS resonator, and cavity optomechanics.

**Mengqiang Zou** was born in Henan, China, in 1990. He received the master's degree in mechanical engineering from the Guilin University of Electronic Technology in 2016. He is currently working toward the Ph.D. degree in optical engineering with Shenzhen University, Shenzhen, China. His major research interests focus on femtosecond laser micromachining and optical fiber sensors.

**Shengzhen Lu** was born in 1997. She received the B.S. degree in physics from Lingnan Normal University, Zhanjiang, China, in 2019. She is currently working toward the master's degree in optical engineering with Shenzhen University, Shenzhen, China. Her major research interests focus on high-Q WGMs resonator.

**Yong Yang** was born in 1979. He received the Ph.D. degree in optics from the University of Science and Technology of China, Hefei, China, in 2008. He was a Postdoctoral Researcher with Oregon University, University College Cork, and Okinawa Institute of Science and Technology Graduate University. His major research interests are optical sensing with whispering gallery mode resonator, nonlinear effect in ultrahigh Q microbubble resonators and development of surface nanoscale axial photonics devices.

**Changrui Liao** was born in Shandong, China, in 1984. He received the B.Eng. degree in optical engineering and the M.S. degree in physical electronics from the Huazhong University of Science and Technology (HUST), Wuhan, China, in 2005 and 2007, respectively, and the Ph.D. degree in electrical engineering from the Hong Kong Polytechnic University, Hong Kong, in 2012. He is currently with Shenzhen University, Shenzhen, China, as an Associate Professor. His current research interests focus on femtosecond laser micromachining, optical fiber sensors, and opto-microfluidics.

**Wenjie Feng** (Senior Member, IEEE) was born in Shangqiu, Henan Province, China, in 1985. He received the B.S. degree from the First Aeronautic College of the Airforce, Xinyang, China, in 2008, the M.Sc., and Ph.D. degrees from the Nanjing University of Science and Technology (NUST), Nanjing, China, in 2010 and 2013, respectively. In 2017, he was a Research Fellow with the City University of Hong Kong, Hong Kong. From 2010 to 2011, he was an exchange student with the Institute of High-Frequency Engineering, Technische Universität München, Munich, Germany. He is currently a Professor with the Nanjing University of Science and Technology, Nanjing, China, and also a Visiting Professor with the South China University of Technology, Guangzhou, China. He has authored or coauthored over 100 IEEE journal papers (including 50 IEEE Transactions papers) and 60 conference papers. His research interests include wideband circuits and technologies, substrate integrated components and systems, planar microstrip filters and power dividers, and LTCC circuits.

**Yiping Wang** (Senior Member, IEEE) was born in Chongqing, China, in 1971. He received the B.Eng. degree in precision instrument engineering from the Xi'an Institute of Technology, China, in 1995 and the M.S. and Ph.D. degrees in optical engineering from Chongqing University, China, in 2000 and 2003, respectively. From 2003 to 2005, he was with Shanghai Jiao Tong University, China, as a Postdoctoral Fellow. From 2005 to 2007, he was with the Hong Kong Polytechnic University, as a Postdoctoral Fellow. From 2007 to 2009, he was with the Institute of Photonic Technology (IPHT), Jena, Germany, as a Humboldt Research Fellow. From 2009 to 2011, he was with the Optoelectronics Research Centre (ORC), University of Southampton, U.K., as a Marie Curie Fellow. Since 2012, he has been with Shenzhen University, Shenzhen, China, as a Distinguished Professor. He has authored or coauthored a book, 21 patent applications, and more than 240 journal and conference papers. His current research interests focus on optical fiber sensors, fiber gratings, and photonic crystal fibers. Prof. Wang is a Senior Member of the Optical Society of America and the Chinese Optical Society.